Journal of Applied Mechanics and Technical Physics, Vol. 39, No. 4, 1998

EXPERIMENTAL AND NUMERICAL INVESTIGATION OF THE DYNAMICS OF UNIFORM TURBULENCE OF A STABLY STRATIFIED FLUID

N. I. Bolonov, V. U. Bondarchuk,[1] I. A. Vatutin,[1]
B. A. Kolovandin,[1] and V. G. Lobachev

UDC 532.517.4

The results of experimental and numerical studies of the dynamics of the parameters of uniform turbulence of a stably stratified fluid for different molecular Prandtl–Schmidt numbers over a wide range of buoyancy times $N\tau$ are given. The tank, the measurement apparatus used, and the experimental procedure are briefly described. The numerical modeling used a second-order model of uniform turbulence of a stratified medium. The influence of fluctuations of the turbulent mass (heat) flux $q(N\tau)$ on the evolution of the statistical parameters of the velocity and temperature fields is analyzed, and an invariant equation is found for the parameters of the strong turbulence of the stratified fluid. It is shown that the statistical parameters of the turbulence, being smoothed with respect to the amplitude of the fluctuations, vary self-similarly with time after the collapse point.

Introduction. The investigation of the evolution of uniform turbulence of a stably stratified fluid is of interest for the development of the general theory of turbulence in a stratified medium. We note that the model of uniform turbulence of a stably stratified fluid describes well the elementary transfer processes occurring in the upper atmosphere and the thermocline region in the ocean. Both experimental studies of liquid and air [2–5] and direct numerical modeling [6–8] have been carried out in recent years to clarify the fundamental properties of the evolution of uniform turbulence of a stably stratified medium, which is described in detail description of which is contained in a monograph [1]. It was shown that a turbulent vertical density flux eventually decreases to zero (conditional collapse of turbulence) and then assumes negative and positive values that alternate with a certain period. It was established by a spectral analysis of data of direct numerical modeling that the contragradient turbulent mass (heat) flux is connected with the conversion of the kinetic energy of pulsations to the potential energy of the density field and is an indication of the substantial contribution of internal gravity waves to the velocity field. In the cited papers, the limited size of laboratory experimental apparatus and the limited technical capabilities of contemporary computers, for reasonable amounts of computer time, prevented the investigation of the evolution of turbulence parameters at sufficiently large values of the turbulent Reynolds number Re and the buoyancy time $N\tau$. The dynamics of uniform turbulence of a stably stratified fluid was investigated numerically in [9] on the basis of a second-order flow model $\langle u_i u_j\rangle - \varepsilon_u - \langle u_i\rho\rangle - \langle\rho^2\rangle - \varepsilon_\rho$ for molecular Prandtl–Schmidt numbers $\sigma = 0.73$ (air) and $\sigma = 900$ (salt water).

The purpose of the present work is an experimental and numerical investigation of the dynamics of uniform turbulence of a stably stratified fluid over a wide range of the parameter σ in a relatively long interval of dimensionless time ($1.25 \leqslant N\tau \leqslant 3$). We set the task of a detailed investigation of the dynamics of statistical turbulence parameters that enter in the second-order flow model.

Donetsk State University, Donetsk 340055. [1]Institute of Heat and Mass Transfer, National Academy of Sciences of Belarusia, Minsk 220072. Translated from Prikladnaya Mekhanika i Tekhnicheskaya Fizika, Vol. 39, No. 4, pp. 64–75, July–August, 1998. Original article submitted August 5, 1996; revision submitted November 10, 1996.

 0021-8944/98/3904-0536 $20.00

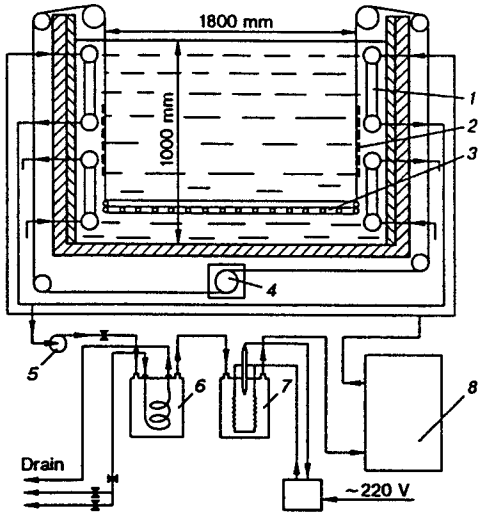

Fig. 1. Diagram of the large tank for studying turbulence behind a grid in a stratified fluid: 1) lateral heat exchanger; 2) textolite plate; 3) grid; 4) electric motor; 5) pump; 6) heat exchanger; 7) thermostat; 8) thermal stabilizing vessel.

1. Experimental Investigation. To investigate the turbulence behind a grid in a stratified medium, we used a water tank with a thermally stratified medium from the Department of Physical Hydrodynamics of Donetsk State University, equipped with nonstandard probes, a hot-wire anemometer for measuring velocity and temperature fields, and a system for data collection, storage, and processing.

The tank (Fig. 1) had dimensions of 12 × 1.2 × 1.8 m, its bottom was made of stainless steel, and the side walls of plate glass. To create quasilinear thermal stratification, we used a scheme with lateral heat exchangers 1. Hot water was passed through the upper heat exchanger and cold water through the lower one. To create stable stratification, each heat exchanger was connected to a circuit consisting of a pump 5, a heat exchanger 6, a thermostat 7, and a thermal-stabilizing vessel 8. The tank walls were carefully insulated to eliminate convection, and the water temperature in the upper layer was kept close to the air temperature at the laboratory. The grid 3 with a size of 2.2 × 1.6 m and a cell size of 92 × 92 mm, made of stainless steel tubing 16 mm in diameter, was lowered into the enclosed section of the tank on four cables fastened to the corners of the grid, and the medium was made turbulent by moving the grid using a special drive 4 mounted below the tank.

Velocity and temperature pulsations in the medium turbulized by the grid were measured by a probe consisting of a horizontally mounted disk. A vertical pylon 60 cm long with three hot-wire anemometer sensors located along it at a 50-mm interval was fastened to the bottom of the disk. The disk was rotated by a transmission and a vibration exciter, at a constant linear velocity of 13.4 cm/sec. Vertical temperature profiles were measured by a resistance thermometer. The rate of probing was 1.59 cm/sec, and the accuracy in measuring the average temperature was ±0.05°C.

To investigate the temperature distribution under the linear stratification conditions, heat exchangers were placed at the surface and at the bottom of the tank, and this prevented us from obtaining large temperature gradients over considerable dimensionless times $N\tau$. We therefore increased the region with a nearly linear temperature distribution by mounting a textolite plate 2 in front of the heat exchangers 1.

We used a direct-current hot-wire anemometer at a carrier frequency to measure velocity and temperature pulsations. The sensors were uninsulated platinum filaments. Two mutually perpendicular filaments 1.5 mm long were placed in a vertical plane at angles of ±45° to the stream. The third (horizontal) filament, connected to the circuit of a resistance thermometer was placed 2 mm in front of the projection of the point of intersection of the inclined filaments. The sensors were produced by etching the copper shell of a Wollaston wire up to the platinum core with a diameter of 8 μm.

The low turbulence intensity and the constancy of the average probe velocity enabled us to use a linear approximation of the hot-wire anemometer calibration curves, which made it possible to reduce the problem of finding the velocity and temperature components to the solution of a system of three equations for instantaneous values of the output voltages of the two hot-wire anemometer channels and the resistance thermometer. Solving this system, we obtain two velocity components $U = A_1e_1 + B_1e_2 - C_1e_3$ and $V = A_2e_1 - B_2e_2 - C_2e_3$ and the temperature $T = De_3$, where e_1, e_2, and e_3 are the instantaneous output voltages of the hot-wire anemometer channels and the resistance thermometer; A_1, A_2, B_1, B_2, C_1, C_2, and D are calibration constants. The pulsation components of the signals were filtered in a 0.6–80 Hz band, amplified to a level of ±5 V, and recorded on a magnetic tape.

We used the method described to investigate the background parameters of velocity and temperature pulsations. The measurements showed that minimum amounts of interference for recording velocity pulsations in the tank were observed at a disk rotation rate $\omega = 0.222$ sec^{-1}, corresponding to movement of the sensors at 0.12–0.14 m/sec. The constant disk rotation rate was set after 1/5 of the first rotation. The nonuniformity of its motion over the rest of the circumference was ±3% of the velocity. The measurement frequency band had a lower limit of 0.6 Hz to reduce the interference from the nonuniformity of disk motion. In the 0.6–80 Hz band the background velocity pulsations together with instrument noise and vibrations comprised no greater than 1 mm/sec in the longitudinal velocity component and 0.5 mm/sec in the vertical component. The standard deviation of the background temperature pulsations (including instrument noise) in a stratified layer with a temperature gradient of 18°C/m was about 0.028°C.

Stable thermal stratification was created in the tank using the lateral heat exchangers. The time of its establishment depended on the initial temperature profile and was 6–10 h. Arrival at the working regime was monitored by measuring vertical temperature profiles in the longitudinal cross section of the tank. After the given temperature distribution was reached, screens were lowered slowly into the water to cover the heat exchangers and prevent the liquid flow through them as the grid was lowered. Then, the temperature-regulating system was turned off and the temperature profile was measured. After about 0.5 h, turbulence was generated by lowering the grid to the bottom of the tank. The time when the grid passed the horizon in which the sensors were located was recorded on the tape. The velocity of the grid was determined from the interruption of a laser beam by a plate of a given length fastened vertically to the grid. The laser beam passed through the working section at the level of the moving sensors. The probe was triggered at a certain time (5–180 sec) after the grid was lowered. Signals from the hot-wire anemometer and pulses from the disk position indicator were recorded on the tape.

Having made a full circle, the sensor entered its own wake and the recording of signals was stopped. The final vertical temperature profile was recorded 5 min after lowering the grid. The temperature-stabilizing system was then turned on to restore the original temperature profile. After 1–2 h the experiment was repeated. We thus accumulated a set of eight to ten realizations with the same time delay.

To obtain sufficiently well-developed turbulence and achieve the longest observation time $N\tau$, we chose the maximum possible grid velocities under the given experimental conditions ($U_\infty = 0.4$ m/sec) and the maximum temperature drop over the tank height. At such a velocity we obtained uniform grid motion in the region of the thermocline in which the measurement were made. The range of short observation times was investigated at reduced temperature drops. The temperature profile was not fully restored over the time between successive experiments, and, hence, the temperature gradients had decreased slightly by the end of the test series. The average temperature gradient in the given test series was used in calculating the stratification parameters.

The turbulence parameters behind the grid were measured at average temperature gradients $dT/dx_2 = 2.9$–12.1°C/m. The Reynolds number $\mathrm{Re}_\infty = U_\infty M/\nu$, calculated for the grid cell size M, was $3.8 \cdot 10^{-4}$–$4.0 \cdot 10^4$, and the Froude number $\mathrm{Fr} = NM/U_\infty$ varied in the range of $1.85 \cdot 10^{-2}$–$3.78 \cdot 10^{-2}$. Data on the investigated regimes are given in Table 1.

Since the background pulsations were due mainly to the nonuniformity of sensor motion, vibrations, and electronic instrument noise, they were assumed to be uncorrelated with turbulent pulsations behind the grid. This enabled us to refine the spectrum of turbulent pulsations by subtracting from the spectrum of the

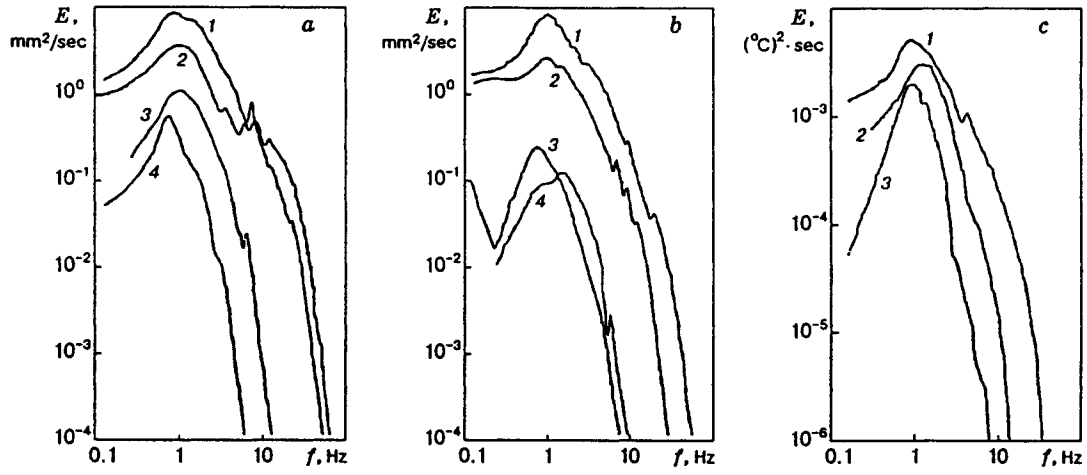

Fig. 2. Spectra of longitudinal (a) and vertical (b) velocity pulsations and temperature pulsations (c) for different stratification regimes: curves 1–4 correspond to regimes 1.1, 1.2, 4.10, and 4.14 (a and b) and curves 1–3 correspond to regimes 2.1, 4.10, and 4.14 (c).

signal of the corresponding spectrum of background pulsations. After subtraction of the "background," the pulsation spectra in the frequency range $f > f_b$ (f_b is the lower boundary of the frequency range) were replaced by the dependence $E(f) \sim f^{-7}$, typical of the range of viscous dissipation. The spectra of longitudinal and vertical velocity pulsations and of temperature pulsations for different regimes of stratification of the medium (see Table 1) are given in Fig. 2.

The results were processed on a personal computer. The instantaneous values of the signals from the outputs of the hot-wire anemometer and the resistance thermometer were converted by the algorithm given above to instantaneous values of the vertical and longitudinal velocity components V and U (relative to the direction of movement of the sensor) and to the instantaneous values of the temperature. The signal was made discrete with a frequency of 256 Hz. From realizations lasting 5 sec we calculated the energy spectra and the second moments of temperature and velocity pulsations. The data obtained were averaged over the set of realizations.

The doubled kinetic energy of the longitudinal (horizontal) velocity pulsations $\langle u_{exp}^2 \rangle = \langle u_1^2 \rangle + \langle u_3^2 \rangle$ and the doubled kinetic energy of transverse (vertical) velocity pulsations $\langle v_{exp}^2 \rangle = \langle u_2^2 \rangle$ were determined separately ($\langle v_{exp}^2 \rangle$ and $\langle u_{exp}^2 \rangle$ are quantities obtained experimentally). Under the conditions of this experiment, we have $\langle u_1^2 \rangle = \langle u_3^2 \rangle$ and $\langle u_{exp}^2 \rangle = 2\langle u_1^2 \rangle$, i.e., the doubled total kinetic energy of the turbulence was determined from the equation

$$\langle q_{exp}^2 \rangle = \langle u_{exp}^2 \rangle + \langle v_{exp}^2 \rangle = \langle u_1^2 \rangle + \langle u_2^2 \rangle + \langle u_3^2 \rangle = \langle q^2 \rangle.$$

The statistical moments of the velocity and temperature pulsations were found from the frequency spectra obtained. Instead of the frequency f, it is more convenient to use the wavenumber $k_1 = 2\pi f/U_\infty$, and instead of $E(f)$ we can introduce the spectral function $E_1(k_1) = U_\infty E(f)/2\pi$. We therefore have $\langle u_1^2 \rangle = \int_0^\infty E_1(k_1)\,dk_1 = \int_{k_{lower}}^{k_{upper}} E_1(k_1)\,dk_1$.

Similarly, we can introduce spectral functions for the transverse velocity pulsations and the temperature pulsations:

$$\langle u_2^2 \rangle = \int_0^\infty E_2(k_1)\,dk_1 = \int_{k_{lower}}^{k_{upper}} E_2(k_1)\,dk_1, \qquad \langle t^2 \rangle = \int_0^\infty E_T(k_1)\,dk_1 = \int_{k_{lower}}^{k_{upper}} E_T(k_1)\,dk_1.$$

TABLE 1

Regime	Re_∞	σ	dT/dt, °C/m	N, sec^{-1}	Fr	x/M	Nr
1.1						71	1.31
1.2						92	1.72
1.3	$3.82 \cdot 10^4$	6.62	2.89	$8.04 \cdot 10^{-2}$	$1.85 \cdot 10^{-2}$	114	2.12
1.4						136	2.52
2.1						66	1.38
2.2						88	1.82
2.3	$3.82 \cdot 10^4$	6.62	3.49	$8.92 \cdot 10^{-2}$	$2.07 \cdot 10^{-2}$	110	2.27
2.4						131	2.72
3.1						132	3.18
3.2						154	3.7
3.3	$3.95 \cdot 10^4$	6.46	4.65	$10.42 \cdot 10^{-2}$	$2.3 \cdot 10^{-2}$	176	4.22
3.4						197	4.74
4.1						135	5.34
4.2						157	6.22
4.3	$4.03 \cdot 10^4$	6.32	12.1	$17.14 \cdot 10^{-2}$	$3.78 \cdot 10^{-2}$	179	7.03
4.4						200	7.91
4.5						272	10.24
4.6						293	11.05
4.7	$4.03 \cdot 10^4$	6.32	10.9	$16.33 \cdot 10^{-2}$	$3.78 \cdot 10^{-2}$	315	11.87
4.8						337	12.69
4.9						401	14.76
4.10						423	15.57
4.11	$4.03 \cdot 10^4$	6.32	10.4	$15.95 \cdot 10^{-2}$	$3.78 \cdot 10^{-2}$	444	16.33
4.12						466	17.14
4.13						578	21.54
4.14						600	22.36
4.15	$4.03 \cdot 10^4$	6.32	10.7	$16.14 \cdot 10^{-2}$	$3.78 \cdot 10^{-2}$	622	23.11
4.16						644	23.93
4.17						836	31.59
4.18						858	32.40
4.19	$4.03 \cdot 10^4$	6.32	11.00	$16.4 \cdot 10^{-2}$	$3.78 \cdot 10^{-2}$	879	33.22
4.20						901	34.04

Here $E_1(k_1)$, $E_2(k_1)$, and $E_T(k_1)$ are the experimentally determined, one-dimensional energy spectra of velocity and temperature pulsations, and k_{lower} and k_u ku are the lower and upper limits of integration.

The rate of dissipation of the kinetic energy of turbulence was estimated from the relation [2]

$$\varepsilon_u^{exp} = \nu\left[10\left\langle\left(\frac{\partial u_1}{\partial x}\right)^2\right\rangle + \frac{5}{2}\left\langle\left(\frac{\partial u_2}{\partial x}\right)^2\right\rangle\right] = \nu\left[10\int\limits_{k_1}^{k_{upper}} k_1^2 E_1(k_1)\,dk_1 + \frac{5}{2}\int\limits_{k_{lower}}^{k_{upper}} k_1^2 E_2(k_1)\,dk_1\right].$$

Similarly, to calculate the rate of "smearing out" of the temperature pulsation gradients, we used the equation

$$\varepsilon_T^{exp} = 6\alpha\int\limits_{k_{lower}}^{k_u} k_1^2 E_T(k_1)\,dk_1.$$

From the results of the measurements we calculated the normalized values of the turbulence parameters:

$$U = \frac{\langle u_1^2\rangle}{U_\infty^2}, \qquad V = \frac{\langle u_2^2\rangle}{U_\infty^2}, \qquad E = \frac{\langle u_1^2\rangle + \langle u_2^2\rangle + \langle u_3^2\rangle}{U_\infty^2},$$

$$\Theta = \frac{\langle t^2\rangle}{(\Delta T)^2}, \qquad \varepsilon_u = \frac{\varepsilon_u^{\exp} M}{U_\infty^3}, \qquad \varepsilon_T = \frac{\varepsilon_T^{\exp} M}{U_\infty (\Delta T)^2}.$$

Here U_∞ is the velocity of the grid and $\Delta T \approx (\partial T/\partial x_2)M$ is the temperature drop over a height equal to the grid cell size M.

The turbulent heat flux $R_{VT} = \langle u_2 t\rangle/(\langle u_2^2\rangle^{1/2}\langle t^2\rangle^{1/2})$ was calculated by a separate program ignoring background pulsations.

2. Numerical Modeling. The model of uniform turbulence of a stratified fluid [9, 10] includes differential equations for the Reynolds stress tensor $\langle u_i u_j\rangle$, the doubled total kinetic energy of the turbulence, $\langle u_i u_i\rangle$ (summation over the recursive indices is presumed here and below), the mean square of pulsations of the density, temperature, or concentration of the admixture $\langle \rho^2\rangle$, the flux vector of the scalar considered $\langle u_i \rho\rangle$, the rate of dissipation of kinetic energy $\varepsilon_u = \nu(-\Delta_\xi \langle u_i u_i'\rangle)_{\xi=0}$, and the rate of "smearing out" of pulsations of the scalar, $\varepsilon_\rho = \alpha(-\Delta_\xi \langle \rho\rho'\rangle)_{\xi=0}$. Along with the calculated parameters, we also consider their associated Taylor macroscopic and microscopic scales:

$$L_u = \frac{5(\langle q^2\rangle)^{3/2}}{\varepsilon_u}, \quad L_\rho = \frac{6(\langle q^2\rangle)^{1/2}\langle \rho^2\rangle}{\varepsilon_\rho}, \quad \lambda_u^2 = \frac{5\nu\langle q^2\rangle}{\varepsilon_u}, \quad \lambda_\rho^2 = \frac{6\alpha\langle \rho^2\rangle}{\varepsilon_\rho}. \tag{2.1}$$

The macroscopic scales are expressed in terms of the corresponding microscopic scales by the equations

$$L_u = \lambda_u \mathrm{Re}, \quad L_\rho = \lambda_\rho \mathrm{Pe}, \quad \mathrm{Re} = \frac{\langle q^2\rangle^{1/2}\lambda_u}{\nu}, \quad \mathrm{Pe} = \frac{\langle q^2\rangle^{1/2}\lambda_\rho}{\alpha}, \tag{2.2}$$

where Re and Pe are the turbulent Reynolds and Peclet numbers. We also introduce the corresponding time scales

$$\tau_u = \frac{\langle q^2\rangle}{\varepsilon_u}, \qquad \tau_\rho = \frac{\langle \rho^2\rangle}{\varepsilon_\rho}. \tag{2.3}$$

It follows from relations (2.1)–(2.3) that the equations for ε_u and ε_ρ can be replaced by equations for the corresponding spatial and time scales (in the authors' opinion, in problems of uniform turbulence it is convenient to use more compact equations for the time scales τ_u and τ_ρ).

The system of differential equations for the turbulence parameters can be represented [9, 10] as

$$\frac{d}{dt}V = -2\left\{\frac{1}{3}\left[d + \frac{9}{2}(1-d)\right]\left(3\frac{V}{E} - 1\right) + \frac{1}{3} + \frac{4}{5}q\frac{T_u}{E}\mathrm{Fr}^2\right\}\frac{E}{T_u}; \tag{2.4}$$

$$\frac{d}{dt}E = -2\left(1 + q\frac{T_u}{E}\mathrm{Fr}^2\right)\frac{E}{T_u}; \tag{2.5}$$

$$\frac{d}{dt}T_u = (F_u - 2) - 2\left[1 - d\left(\frac{2\sigma}{1+\sigma}\right)\left(\sigma_{Tawo} + \frac{3}{5}\right)\frac{1}{R_{awo}}\frac{T_u}{T_\rho}\right]\mathrm{Fr}^2 q\frac{T_u}{E}; \tag{2.6}$$

$$\frac{d}{dt}q = -\left[\frac{2}{3} - \frac{1}{\mathrm{Fr}^2}\frac{V}{\Theta} - d\left(\frac{V}{E} - \frac{1}{3}\right)\right]\mathrm{Fr}^2\Theta - \left[(1-d)\left(\frac{1}{3} + 25\frac{V}{E}\frac{T_u}{T_\rho}\right) + 2d\left(\sigma_{Tawo} + \frac{3}{5}\right)\frac{1}{R_{awo}}\frac{T_u}{T_\rho}\right]\frac{q}{T_u}; \tag{2.7}$$

$$\frac{d}{dt}\Theta = -2\left(1 - q\frac{T_\rho}{\Theta}\right)\frac{\Theta}{T_\rho}; \tag{2.8}$$

$$\frac{d}{dt}T_\rho = (F_{\rho 2} - 2) + F_{\rho 1}\frac{T_\rho}{T_u} - d\frac{4}{3}\left(1 - \frac{3}{5R_{awo}}\right), \tag{2.9}$$

where the following notation is adopted:

$$t = \frac{\tau U_\infty}{M}, \quad T_u = \frac{\tau_u U_\infty}{M}, \quad T_\rho = \frac{\tau_\rho U_\infty}{M}, \quad V = \frac{\langle u_2^2\rangle}{U_\infty^2}, \quad E = \frac{\langle q^2\rangle}{U_\infty^2}, \quad q = \frac{\langle u_2\rho\rangle}{U_\infty M(-d\langle\rho\rangle/dx_2)},$$

$$\Theta = \frac{\langle \rho^2\rangle}{M^2(-d\langle\rho\rangle/dx_2)^2}, \quad \sigma_{Tawo} = \frac{3}{10}\left(\frac{1-\sigma}{\sigma}\right)\left[1 - \left(\frac{2\sigma}{1+\sigma}\right)^{3/2}\right]^{-1},$$

$$R_{awo} = \frac{1}{5\sigma}\left[1 - 2\left(\frac{2\sigma}{1+\sigma}\right)^{3/2} + \sigma^{3/2}\right]\left[1 - 2\left(\frac{2\sigma}{1+\sigma}\right)^{1/2} + \sigma^{1/2}\right]^{-1},$$

$$F_u = F_{us}(1-d) + F_{uw}d, \quad F_{us} = \frac{11}{3}, \quad F_{uw} = \frac{14}{5}, \quad d = 1 - 2\left(1 + \sqrt{1 + \delta_u/\mathrm{Re}^2}\right)^{-1},$$

$$\delta_u = 2.8 \cdot 10^3, \quad \mathrm{Re}^2 = 5\mathrm{Re}_\infty E T_u, \quad \mathrm{Re}_\infty = \frac{U_\infty M}{\nu}, \quad F_{\rho 1} = F_u - 2 - \frac{4}{5}d, \quad F_{\rho 2} = 2 + \frac{4}{3}d, \quad \mathrm{Fr} = \frac{NM}{U_\infty}.$$

This system of equations was solved numerically. The initial conditions were taken from the experiments with appropriate correction for their self-consistency with respect to all the calculated parameters.

3. Comparison of Numerical and Experimental Results. The normalized parameters U, V, E, and Θ used in the numerical modeling coincide with the corresponding experimental parameters. The normalized turbulent heat flux q is related to the experimental coefficient of correlation of the velocity and temperature pulsations $q = -R_{VT}V^{1/2}\Theta^{1/2}$, and the normalized time scales T_u and T_ρ are defined in terms of experimental parameters as $T_u = E/\varepsilon_u$ and $T_\rho = \Theta/\varepsilon_T$. The dimensionless time of evolution $t = \tau U_\infty/M$ in Eqs. (2.4)–(2.9) is related to the buoyancy time $N\tau$ by the relation $t = N\tau/\mathrm{Fr}$.

Strong, evolving, uniform turbulence has been investigated earlier in experiments with salt water ($\sigma = 900$) [4] and air ($\sigma = 0.73$) [5]. In the present work we performed an experiment on ordinary water with a constant temperature gradient for $\sigma = 6.5$, $\mathrm{Fr} = (2.0\text{–}3.78) \cdot 10^{-2}$, and $M = 9.2 \cdot 10^{-2}$ m. This enabled us to obtain additional data for a molecular Prandtl number intermediate between the experimental values indicated above. The main difference in the experiment presented here consists in the longer time of observation of the turbulence parameters owing to the use of a large test tank. The dimensionless time of evolution $N\tau$ in [4] did not exceed 2.6, and in [5] it did not exceed 2.0, whereas in our experiment the maximum $N\tau$ was 34.0. The investigation of the evolution of turbulence parameters thus covers different stages both before and after the onset of conditional collapse of the vertical turbulent heat flux (by conditional collapse we mean the state of turbulence that corresponds to the first zero value of the turbulent mass flux).

Figure 3 gives experimental data from the present work for $\sigma = 6.62$, data from [5] for $\sigma = 0.73$ and data from [4] for $\sigma = 900$, and also results of numerical modeling. The turbulent flux of the scalar quantity q (Fig. 3a), which determines the source terms in the equations for V, E, and T_u, undergoes oscillations about the position $q = 0$, with zero value first reached at $N\tau = 2.5\text{–}3.0$. The oscillation period is estimated to be $T \approx 0.52T_{BV}$ (T_{BV} is the Brunt–Väisälä period, equal to $2\pi/N$), and does not depend on the Prandtl number. The alternation in time of "natural" and "contragradient" mass (heat) fluxes is a fundamental property of uniform turbulence of the type under consideration, indicating active exchange between the kinetic energy of the velocity field and the potential energy of the density field. As is well known from [7, 8], such exchange leads to the generation of internal gravity waves in the turbulent medium and the formation of a mixed velocity field. The results of the modeling performed here show that this property is inherent to flows with any Brunt–Väisälä frequency N, no matter how low. As we showed in [9], however, the amplitude of oscillations of this function decreases with decrease in the molecular Prandtl number. As regards the experimental confirmation of this property, one must bear in mind that for small σ, the amplitude of oscillations of q is within the confidence interval of measurement, which complicates the determination of the oscillations directly from experiment. However, the results of the present work (Fig. 3a), obtained at evolution times after conditional collapse, confirm the presence of oscillations. The alternation of the sign of q, which is not evident in Fig. 3a at the adopted linear scale along the ordinate axis, is confirmed by the numerical values of a number of points on the abscissa axis.

The oscillations of the function q cause oscillations of the kinetic energy of vertical pulsations of the velocity V (Fig. 3b), which in turn results in oscillations of the total kinetic energy E of the turbulence. Oscillations of the average horizontal pulsations of velocity U are less noticeable, since for them the stratification effect is manifested not directly but only by means of the exchange of the energies of the velocity components due to pressure pulsation.

Note that the absence of vertical turbulent mass (heat) transfer at $N\tau \approx 30$, observed in Fig. 3a, does not indicate suppression of the velocity pulsations, which, as follows from Fig. 3b, die out at an average (in oscillation amplitude) rate not exceeding the rate of degeneration of velocity pulsations of an unstratified fluid.

The oscillations of the function q also affect the behavior of the density pulsations Θ (Fig. 3c). At

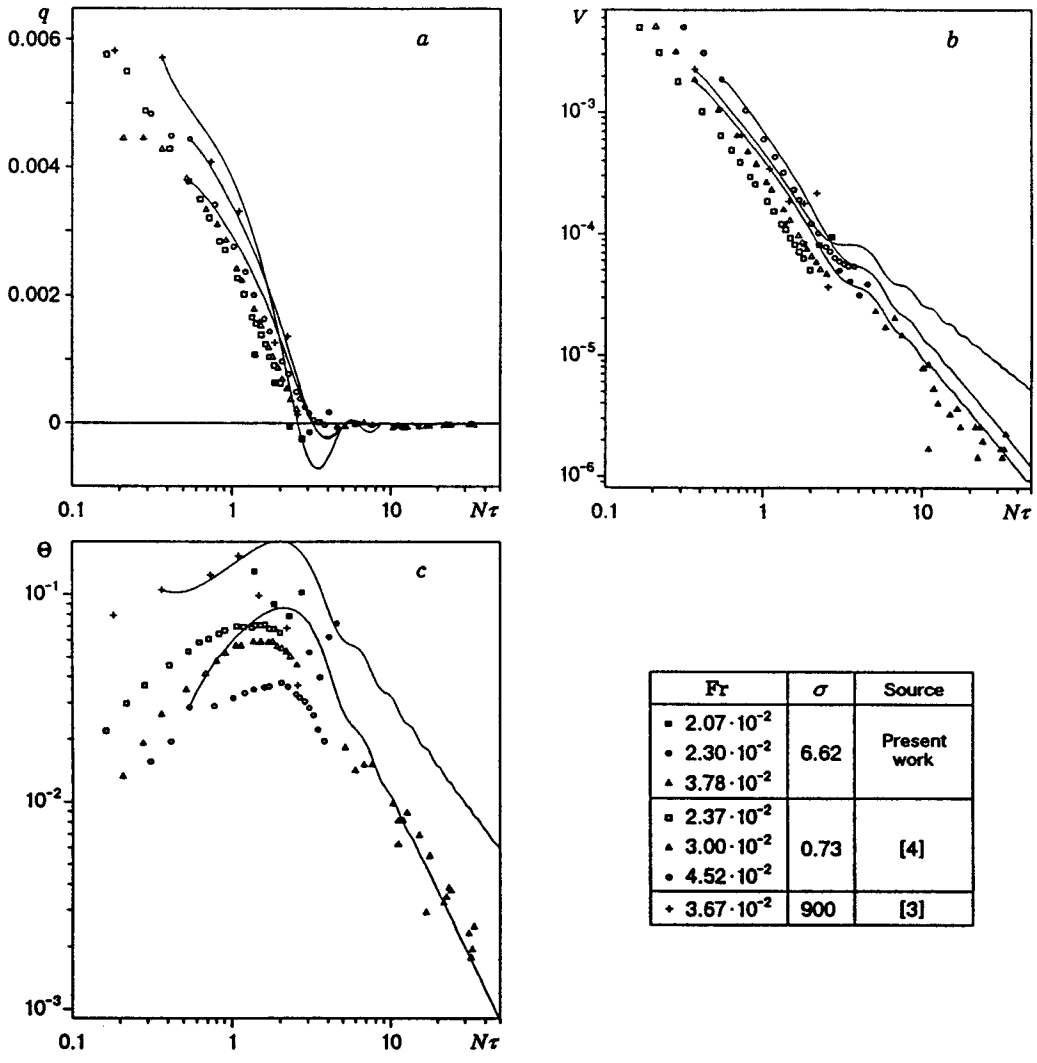

Fr	σ	Source
▪ 2.07·10⁻² • 2.30·10⁻² ▲ 3.78·10⁻²	6.62	Present work
▫ 2.37·10⁻² ▲ 3.00·10⁻² • 4.52·10⁻²	0.73	[4]
+ 3.67·10⁻²	900	[3]

Fig. 3. Dynamics of transverse turbulent heat flux (a), transverse velocity pulsations (b), and temperature pulsations (c) for different Froude numbers and molecular Prandtl numbers: solid curves are the result of numerical modeling.

$N\tau < 1$, the parameter Θ varies just like a passive scalar in uniform turbulence [11], and at $N\tau \approx 2.5$ it starts to die out, qualitatively similar to the damping of an isotropic passive scalar. A feature of the evolution of the dispersion of Θ, in contrast to the isotropic case, is its oscillatory nature with a period equal to the period of oscillations of the vertical turbulent mass (heat) flux.

The oscillatory changes in the turbulence parameters in a medium with stable density stratification indicate the presence of internal waves in the total field excited by gravitational forces. It can be assumed that at $N\tau \approx 1$, the contribution of random internal waves to the superposed velocity field becomes comparable to the contribution of turbulence itself. Starting with this value of $N\tau$, one should expect that the dynamics of the parameters considered shows typical features of the turbulence of a stratified fluid. In fact, for $N\tau = 2.5$–3.0, corresponding to conditional collapse of the turbulent mass (heat) flux, one observes an abrupt decrease in the rate of decay of velocity pulsations (see Fig. 3b). This is obviously caused by the generation of relatively low-frequency internal waves, which dissipate more slowly than the turbulence itself (this question is discussed in more detail in [12]).

4. Influence of the Molecular Prandtl Number. As follows from Fig. 3, in the near region ($N\tau \leqslant 1$), where the influence of buoyant forces on the field of velocity pulsations is slight, the turbulence

parameters behave similarly to the case of a passive scalar. The parameters of the velocity field evolve self-similarly and do not depend on the molecular Prandtl number σ. The dynamics of the parameters of a scalar field, particularly the quantities Θ and T_ρ, is determined by the initial values of the scale ratio $R^0 = T_u^0/T_\rho^0$, which differ considerably from each other in experiments on air and water. In other words, the difference in the exponents in the laws of evolution of the turbulence parameters for the scalar field in the vicinity of $N\tau \leqslant 1$ is due to a difference not in values of σ but in the initial scale ratio R^0. An analysis of system (2.4)–(2.9) leads to the same conclusion. In the near region ($N\tau \leqslant 1$), the turbulence is strong (the turbulent Reynolds number is large, $\mathrm{Re} \gg 1$). Here the parameter d is practically zero. Thus, the clear dependence of the turbulence parameters determined by this system of equations on the molecular Prandtl number disappears.

We should note that from Eqs. (2.5), (2.6), and (2.9) in the limiting case of strong turbulence (for $d = 0$) we obtain the equations

$$\frac{T_u}{E}\frac{d}{dt}(E/T_u) = -\frac{11}{3T_u}, \qquad \frac{3}{5T_\rho}\frac{dT_\rho}{dt} = \frac{1}{T_u}. \tag{4.1}$$

The solution of system (4.1) leads to the invariant

$$ET_\rho^{11/5}/T_u = \text{const}. \tag{4.2}$$

In the case of a passive scalar with $\mathrm{Re} \gg 1$, the conditions $R = T_u/T_\rho = \text{const}$ are satisfied and relation (4.2) becomes the well-known Saffman's invariant [13]

$$ET_u^{6/5} = \text{const}. \tag{4.3}$$

Thus, relation (4.2) should be treated as a generalization of Saffman's invariant to the case of strong ($\mathrm{Re} \gg 1$) uniform turbulence of a stably stratified fluid.

The results of the experiment described and the numerical modeling at $N\tau > 1$ pertain to moderately strong turbulence of the velocity field. At the same time, the turbulence of the scalar field is moderately strong for $\sigma \approx 1$ and quite strong (the turbulent Peclet number is large, $\mathrm{Pe} \gg 1$) for $\sigma \gg 1$. In this connection it can be expected that even for approximately equal Froude numbers but for considerably different molecular Prandtl numbers, the dynamics of the turbulence parameters will differ considerably.

In the region of conditional collapse, as noted above, there is an abrupt qualitative change in the turbulence parameters under the influence of internal gravity waves. After this, the statistical parameters of the velocity field, being smoothed in oscillation amplitude, vary "self-similarly." The rates of conditionally self-similar evolution of the corresponding parameters differ considerably for $\sigma \approx 1$ and $\sigma \gg 1$, however. It follows from Fig. 3b, for example, that the exponent n of the decay rate of the kinetic energy of vertical pulsations averaged over the oscillation amplitude in the power law $V \sim (N\tau)^{-n}$ is approximately 0.8 for salt water ($\sigma = 900$) and 1.63 for air ($\sigma = 0.73$). The relatively low decay rate for V in the case of $\sigma \gg 1$ may be due to the larger contribution of the energy of internal gravity waves, capable of producing relatively larger-scale and hence more slowly dissipating inhomogeneities than in the case of σ on the order of 1.

The molecular Prandtl number also affects the decay of scalar pulsations, and starting with $N\tau$ corresponding to conditional collapse, the rates of decay of the parameters V and Θ averaged over the oscillation amplitude prove to be the same for the same σ (see Fig. 3c).

For salt water ($\sigma \gg 1$), conditional collapse of the vertical turbulent mass flux occurs at a smaller value of $N\tau$ than for a fluid with $\mathrm{Pr} \approx 1$ (see Fig. 3a). We can conclude that the amplitude of oscillations of the parameter q increases with increase in the Prandtl number.

Conclusion. The satisfactory agreement between the results of numerical modeling and experimental data over a broad range of buoyancy times $N\tau$ suggests that the use of the second-order flow model is efficient in the investigation of the parameters of the superposed field of intrinsic turbulence and internal waves. This model enables one to analyze the dynamics of uniform turbulence of a stably stratified fluid over a wide range of molecular Prandtl numbers, not presently accessible either to experimental investigation or to direct numerical modeling (see, e.g., [7, 8, 14]).

As a result of the present investigation, we can draw the following conclusions:

(1) A fundamental feature of the evolution of the uniform turbulence of a stratified fluid is the oscillatory, sign-changing variation of cross correlation $\langle u_2\rho\rangle$ with a period approximately equal to half the Brunt–Väisälä period (alternation in time between gradient and contragradient mass fluxes).

(2) The value of the turbulent mass (heat) flux averaged over the oscillation amplitude in the investigated range of buoyancy times for Froude numbers of the order of 10^{-2} (see Fig. 3a) is contragradient for all investigated values of σ and approaches zero with increase in the buoyancy time $N\tau$.

(3) In the near region, i.e., up to the buoyancy time that corresponds to conditional collapse of the turbulent scalar flux, the parameters of the mixed field vary with time almost independently of the molecular Prandtl number. The well-known Saffman's invariant for strong ($\mathrm{Re} \gg 1$) uniform turbulence was generalized to the case of a stably stratified fluid with a constant vertical gradient of the averaged density.

(4) Starting with the value of $N\tau$ that corresponds to the conditional collapse of the turbulent scalar flux, there is an abrupt change in the exponents in the power laws of evolution of all the statistical turbulence parameters averaged over the oscillation amplitude. The final stage, which corresponds to $\mathrm{Re} \ll 1$ and $\mathrm{Pe} \ll 1$, was analyzed in a monograph [1].

This work was supported by the International Science Foundation (Grant No. MX 2000) and the Belarusian Foundation for Fundamental Research (Grant No. T14-130).

REFERENCES

1. B. A. Kolovandin, I. A. Vatutin, and V. U. Bondarchuk, *Modeling of Uniform Turbulence of a Stratified Fluid* [in Russian], Phys.-Tech. Inst., National Acad. of Sci. of Belarusia, Minsk (1997).
2. T. D. Dickey and G. L. Mellor, "Decaying turbulence in neutral and stratified fluids," *J. Fluid Mech.*, **89**, 13–31 (1980).
3. D. S. Stillinger, K. N. Helland, and C. W. Van Atta, "Experiments on the transition of homogeneous turbulence to internal waves in a stratified fluid," *J. Fluid Mech.*, **131**, 91–122 (1983).
4. E. C. Itsweire, K. N. Helland, and C. W. Van Atta, "The evolution of grid-generated turbulence in a stably stratified fluid," *J. Fluid Mech.*, **162**, 299–338 (1986).
5. J. H. Lienhard and C. W. Van Atta, "The decay of turbulence in thermally stratified flow," *J. Fluid Mech.*, **210**, 57–112 (1990).
6. J. J. Riley, R. W. Metcalfe, and M. A. Weissman, "Direct numerical simulation of homogeneous turbulence in density stratified fluids," in: *Nonlinear Properties of Internal Waves*, AIP Conf. Proc., Vol. 76, La Jolla Institute (1981), pp. 79–112.
7. O. Metais and J. R. Herring, "Numerical simulations of freely evaluating turbulence in stably stratified fluids," *J. Fluid Mech.*, **202**, 117–148 (1989).
8. S. E. Holt, J. R. Koseff, and J. H. Ferziger, "A numerical study of the evolution of structures of homogeneous stably stratified sheared turbulence," *J. Fluid Mech.*, **237**, 499–511 (1992).
9. B. A. Kolovandin, V. U. Bondarchuk, C. Meola, and G. De Felice, "Modeling of the homogeneous turbulence dynamics of stably stratified media," *Int. J. Heat Mass Transfer*, **36**, 1953–1968 (1993).
10. B. A. Kolovandin, "Modeling the dynamics of turbulent transport processes," *Adv. Heat Transfer*, **21**, 185–237 (1991).
11. V. U. Bondarchuk, B. A. Kolovandin, and O. G. Martynenko, "Modeling of developing nearly homogeneous turbulence of velocity and scalar fields," *Int. J. Heat Mass Transfer*, **34**, 11–30 (1991).
12. B. A. Kolovandin and I. A. Vatutin, "Study of the final evolution of homogeneous turbulence in density stratified fluid," in: *Turbulent Shear Flows, Proc. of the 10th Symp.*, Vol. 10 (1995), p. 6.
13. P. G. Saffman, "The large-scale structure of homogeneous turbulence," *J. Fluid Mech.*, **27**, 581–588 (1967).
14. T. Gerz and H. Yamazaki, "Direct numerical simulation of buoyancy-driven turbulence in stably stratified fluid," *J. Fluid Mech.*, **249**, 415–440 (1993).